



Article

Comparison of Field and SAR-Derived Descriptors in the Retrieval of Soil Moisture from Oil Palm Crops Using PALSAR-2

Veena Shashikant ¹, Abdul Rashid Mohamed Shariff ^{1,2,3,*}, Aimrun Wayayok ^{1,2,3}, Md Rowshon Kamal ¹, Yang Ping Lee ⁴ and Wataru Takeuchi ⁵

¹ Department of Biological and Agricultural Engineering, Faculty of Engineering, Universiti Putra Malaysia, Serdang 43400, Malaysia; gs52191@student.upm.edu.my (V.S.); aimrun@upm.edu.my (A.W.); rowshon@upm.edu.my (M.R.K.)

² SMART Farming Technology Research Center, Faculty of Engineering, Universiti Putra Malaysia, Serdang 43400, Malaysia

³ Laboratory of Plantation System Technology and Mechanization, Institute of Plantation Studies, Universiti Putra Malaysia, Serdang 43400, Malaysia

⁴ FGV R&D Sdn Bhd, Level 9, Wisma FGV, Jalan Raja Laut, Kuala Lumpur 50350, Malaysia; yangp.lee@fgvholdings.com

⁵ Department of Human and Social Systems, Institute of Industrial Science, The University of Tokyo, Tokyo 153-8505, Japan; wataru@iis.u-tokyo.ac.jp

* Correspondence: rashidpls@upm.edu.my; Tel.: +60-39769-6414



Citation: Shashikant, V.; Mohamed Shariff, A.R.; Wayayok, A.; Kamal, M.R.; Lee, Y.P.; Takeuchi, W. Comparison of Field and SAR-Derived Descriptors in the Retrieval of Soil Moisture from Oil Palm Crops Using PALSAR-2. *Remote Sens.* **2021**, *13*, 4729. <https://doi.org/10.3390/rs13234729>

Academic Editors: Takeo Tadono and Masato Ohki

Received: 14 September 2021

Accepted: 5 November 2021

Published: 23 November 2021

Publisher's Note: MDPI stays neutral with regard to jurisdictional claims in published maps and institutional affiliations.



Copyright: © 2021 by the authors. Licensee MDPI, Basel, Switzerland. This article is an open access article distributed under the terms and conditions of the Creative Commons Attribution (CC BY) license (<https://creativecommons.org/licenses/by/4.0/>).

Abstract: Synthetic-aperture radar's (SAR's) capacity to resolve the cloud cover concerns encountered while gathering optical data has tremendous potential for soil moisture data retrieval using SAR data. It is possible to use SAR data to recover soil moisture because the backscatter coefficient is sensitive to both soil and vegetation by penetrating through the vegetation layer. This study investigated the feasibility of employing a SAR-derived radar vegetation index (RVI), the ratios of the backscatter coefficients using polarizations of HH/HV ($R_{HH/HV}$) and HV/HH ($R_{HH/HV}$) to an oil palm crops as vegetation indicators in the water cloud model (WCM) using phased-array L-band SAR-2 (PALSAR-2). These data were compared to the manual leaf area index (LAI) and a physical soil sampling method for computing soil moisture. The field data included the LAI input parameters and, more importantly, physical soil samples from which to calculate the soil moisture. The fieldwork was carried out in Chuping District, Perlis State, Malaysia. Corresponding PALSAR-2 data were collected on three observation dates in 2019: 17 January, 16 April, and 9 July. The results showed that the WCM modeled using the LAI under HV polarization demonstrated promising accuracy, with the root mean square error recorded as $0.033 \text{ m}^3/\text{m}^3$. This was comparable to the RVI and $R_{HH/HV}$ under HV polarization, which had accuracies of 0.031 and $0.049 \text{ m}^3/\text{m}^3$, respectively. The findings of this study suggest that SAR-based indicators, $R_{HH/HV}$ and RVI using PALSAR-2, can be used to reduce field-related input in the retrieval of soil moisture data using the WCM for oil palm crop.

Keywords: leaf area index; leave-one-out cross-validation; oil palm; radar vegetation index; synthetic aperture radar; soil moisture; vegetation descriptors; water cloud model

1. Introduction

Oil palm has long been recognized as a vital crop in tropical agricultural regions with a consistently increasing output rate, especially in Indonesia and Malaysia, which export significant amounts of crude palm oil to other countries [1]. In Malaysia, oil palm crop production occupies 71% of the agricultural land [2]. Oil palm crop is the second most important source of edible oil, behind soybean, in terms of production [3]. Beyond its core role as an edible oil, palm oil has spawned other palm-based sectors, such as specialized fats, cocoa-butter alternatives, oleochemicals, soaps, domestic detergents, nutritional

supplements and, most recently, bioenergy [4]. Tropical regions like Malaysia that have sufficient rainfall and sunshine and appropriate soil conditions are ideal for oil palm cultivation [5]. Because of the increasing demand for palm oil, a major concern is maintaining crop yields at optimum levels and minimizing labor and fertilizer usage [6]. Due to the fact that the crops in oil palm plantations are linked directly with the ground, soil quality is an important factor when it comes to crop uptake and health [7]. Soil characteristics and climatic conditions are known to vary on a minute scale and are particularly site specific [8].

It has been well established that soil moisture and precipitation have the highest correlations in arid and dry regions and weaker correlations in wet regions, indicating that soil moisture and precipitation are more complex than what is viewed on the surface [9]. The intricate interaction between soil moisture and precipitation has been noted as important in the land-surface context. Correlations between precipitation and soil moisture are the strongest in areas with sparse vegetation, whereas forests and heavily vegetated areas have weaker correlations [10]. Understanding this enables study to focus on numerous specific scientific challenges such as subsurface recharge assessment and the identification of drought–flood cycles. Such studies are important for tropical countries—particularly agricultural nations where widespread applications are possible for scheduled irrigations and soil moisture modeling [11]. However, a lack of information on such topics makes it difficult for the farmers in those countries to take appropriate precautions to ensure the productivity of their crops. Furthermore, hydrological models are often developed for use under static conditions [12]. Additionally, in areas where oil palms are cultivated, soil moisture is equally important for supporting palm tree growth. Therefore, in order to estimate soil moisture by conventional means, highly reliable gravimetric measurements are taken, although this is regarded as time and resource intensive [13]. In response to this, time–domain reflectometry sensors are widely preferred [14], which can provide continuous measurements [15].

Soil moisture mapping is accomplished mostly through extensive point measurements, which can be expensive [16]. Numerous interpolation techniques have been used to produce gridded soil moisture data from field observations, including deterministic approaches such as inverse distance weighting (IDW), local polynomial interpolation (LPI) and radial basis function (RBF) as well as geostatistical methods such as ordinary kriging (OK) [17]. Deterministic methods can be examined using measured points evaluated based on their extent of similarity. It has been noted that model IDW, using soil moisture, is capable of investigating the distribution of drought conditions [18]. When precipitation is encountered on a catchment scale, it has been found that IDW, with the inverse distance to a power number, has a greater impact on simulated outcomes than the scale of grid sampling [19]. In a separate case, the evaluation of soil moisture using deterministic methods, such as IDW and RBF, using global polynomial interpolation, LPI and OK, have been examined, with OK being found to be more effective due to the fact of its use of geostatistical interpolation techniques that utilize the statistical properties of the measured points [20]. As it reduces the variance of estimate error, OK is the most used geostatistical interpolation approach and the best linear unbiased estimator [21]. In complicated terrains, OK is highly dependent on the homogeneity and density of the soil samples [22]. Recently, the topic of soil moisture has concentrated on the spatial and temporal variability of the moisture content in hillslopes and catchments. Fluctuations in soil moisture on slopes are more complicated because of the synergy and superposition effects of land use types, slope gradient, slope aspect, slope position, and elevation [23]. Hilly areas often face the problem of sparse rain gauge networks, which limits the accessibility of the data and affects the interpolation accuracy [24]. Therefore, using remote sensing as a tool, satellite imagery can provide useful information about the Earth's surface, with images being one of the most popular data sources for remote sensing.

Remote sensing is used in the oil palm industry in tree detection [25], monitoring for pests and disease mapping [26], and in nutrient detection [27]. Optical imaging gathers energy emitted from the surface of the Earth in the visible and near-infrared range [28],

resulting in indices that represent the vegetation cover. The normalized difference vegetation index (NDVI), which is a normalized ratio of near-infrared to visible red, is the most commonly used metric [29]. It is a flexible and an effective indicator for distinguishing vegetation from non-vegetation and includes the ability to interpret the health of oil palm trees [30].

On the other hand, microwave remote sensing, or active remote sensing, can produce images regardless of weather or lighting conditions by using its own radiation for illumination, which can penetrate clouds and reach the Earth's surface. Microwave remote sensing has addressed the issue of cloud cover through optical sensors in remote sensing [31], clouds being a major impediment, particularly in tropical areas where oil palms are commonly cultivated [32]. Microwave remote sensing using PALSAR-2 generates data based on backscattered radiation from the ground, with a lengthier wavelength providing better penetrative capability [33]. As the radar has better penetrative capacity, it can be used to distinguish a smooth surface from a rough surface [34]. L-band SAR imagery provides the optimum diagnostic of oil palm canopies for growth monitoring [35]. As a result, the L band at a wavelength of 15–30 cm can penetrate tree canopies and offer information on sub-canopy structures [36]; hence, because of this capability, SAR can be employed in the categorization of oil palms.

Various types of information about the surface can be obtained from the vegetation cover by studying the polarization of the emitted and received radar signal. In HH, the signal is horizontally emitted and horizontally received; in HV, it is horizontally emitted and vertically received; in VH, it is vertically emitted and horizontally received; in VV, it is vertically emitted and vertically received [37]. Polarimetric SAR is a technique used to extract information from vegetation, with important information for oil palm crop categorization being carried by HH and HV signals [38]. In order to distinguish oil palm cover from natural forest and acacia plantations, both the C band and L band can be used to enhance the classification accuracy [39]. Moreover, using an optical sensor, object-based classification was used to improve classification accuracy in oil palm and acacia plantations [40]. Recently, SAR images have been shown to be capable of penetrating oil palm trunks, where basal root disease can be distinguished using a machine-learning model [41].

In the last decade, a better understanding of SAR has allowed the retrieval of soil moisture data from woody plants [42] and agricultural crops [43,44] using vegetation and soil parameters and the water cloud model (WCM). The WCM was proposed as a collection of similar spherical particles that are consistently distributed across the volumetric vegetation layer [45]. Originally, the WCM established an equation for the total backscatter coefficient as a function of soil volumetric moisture content, vegetation moisture content, and plant height [45]. Field-based vegetation parameters, such as the LAI [46–49] and vegetation water content [50,51], have been widely used in WCMs. The WCM has the advantage of being able to explain complicated scatter patterns in a vegetated area using simple bulk vegetation descriptors [52]. However, there is a lack of understanding or agreement on the best collection of vegetation descriptors. Recent studies have shown that using the NDVI [53], based on optical images and the radar vegetation index (RVI) [54,55], and the ratio of backscatter coefficient polarization (e.g., HH/VV [56] or VH/VV [56,57]) as descriptors provides successful soil moisture data retrieval in both the C and L bands. However, HV/HH has been used to understand the dynamics of soil moisture based on radar data, which lessens the effect of soil surface roughness [58]. The HV backscatter coefficient has been found to be sensitive, in the P and L bands, to plant biomass and plant water content [59].

In this study, the main goal was to extract soil moisture data from the oil palm cultivated site using the WCM and SAR-based vegetation descriptors, such as RVI and the ratio of the backscatter coefficients HH/HV ($R_{HH/HV}$) and HV/HH ($R_{HV/HH}$), and compare this with data from the LAI field-based vegetation descriptor.

2. Study Area and Materials

2.1. Study Area

Chuping, in Perlis State, is a flat-terrain oil palm growing location. For this study, the area of the oil palm crop was approximately 28 ha. As of the data collection date, it covered 4-year-old palm stands that had just begun to bear fresh oil palm fruits. The study area's central coordinates were 6°31'07.2" N, 100°19'07.7" E, located in the subdistrict called Kilang Gula Chuping. The area has a relatively flat terrain with a slope angle of 4–12% and an elevation of 21.6 m. The soil type was identified as Chuping and Dampar—sandy clay loam and clay loam. The study was conducted over three periods during weather conditions similar to those in which the SAR images were acquired (see Section 2.2.2). Early in the year, precipitation rates were quite low. This was particularly true in January–March, which are considered to be the driest months of the year, according to meteorological data from a previous study conducted in the same area [60]. The latter months of the year experienced sufficient precipitation, with the average precipitation being 1362.38 mm per year [61].

2.2. Data Collection

2.2.1. Field Data

In order to determine the soil moisture content at a depth of 0–5 cm, a soil gravimetric technique was used in a grid point shown in Figure 1. For this, fresh weights of soil were taken in the field, with their dry weights being calculated in the laboratory, following oven drying. The soil samples were obtained from 32 locations in the study area, resulting in 96 soil samples taken on three different dates. In addition, oil palm fronds were collected for estimation of the LAI. For oil palm crop, the standard approach of destructive sampling was used to determine the LAI. In addition to being an excellent predictor of a palm's nutritional condition, fronds are easy to identify and sample. In oil palm crop, using the 17th frond is widely accepted to estimate LAI [62]. According to the conventional method for evaluating LAI, which was developed specifically for oil palm crop, it was determined using the variables A_f as leaf area per frond in m^2 of the 17th frond from the palm crown, F_n as the total number of fronds per sampled tree, and P_{DEN} as the number of palm trees per hectare, using the following equation [63]:

$$LAI \left(m^2/m^2 \right) = A_f \times F_n \times \frac{P_{DEN}}{10000} \quad (1)$$

The leaflet area was measured using an LI-3100C area meter (LI-COR Inc., Lincoln, NE, USA). The total leaflet area of each frond was calculated by multiplying one side of the leaflet area by two.

2.2.2. Remote Sensing Data

The backscatter coefficient of the oil palms was extracted using PALSAR-2 data. High-resolution PALSAR-2 images were collected through our participation with the Japanese Aerospace Exploration Agency (JAXA) using the Earth Observation Research Announcement 2 platform. Three 2019 PALSAR-2 images, from the HH and HV polarization on 17 January, 19 April, and 9 July, were used. The specifics of these SAR data are shown in Table 1, with all three images having been acquired in Strip Map 3 mode, in ascending order at 6.25×6.25 m resolution. All the PALSAR-2 images used in this study were constructed using a 16 bit data type with each pixel containing a digital number (DN). These DNs did not correspond to the radar signal of the ground features or objects. As a result, the DNs had to be converted into backscatter coefficients and expressed in decibels, as described in Equation (2). For the PALSAR-2 data provided by JAXA, the calibration factor (CF) was -83.0 dB [64]:

$$\sigma^0 = 10 \times \log_{10} \left(DN^2 \right) + CF \quad (2)$$

Once the σ_{HH}^0 and σ_{HV}^0 for each field point were available, the images were radiometrically calibrated using the Shuttle Radar Topography Mission's digital elevation model (3 arc-second). Following that, the images were orthorectified with respect to geographic locations in order to eliminate speckles and noise from the PALSAR-2 images; a Lee filter was used with a 5×5 window size. It has been previously noted that the Lee filter works very well in terms of maintaining an image's spectral characteristics while decreasing speckling [65]. The open-source Sentinel Application Platform version 6.0.0 was used to commence all the SAR-related preprocessing presented in Table 1.

Table 1. PALSAR-2 satellite image acquisition and incident angle.

Date of Acquisition	Polarization	Incident Angle
17 January 2019	HH + HV	30.4–42.4°
19 April 2019	HH + HV	41.2–53.3°
9 July 2019	HH + HV	30.4–42.4°

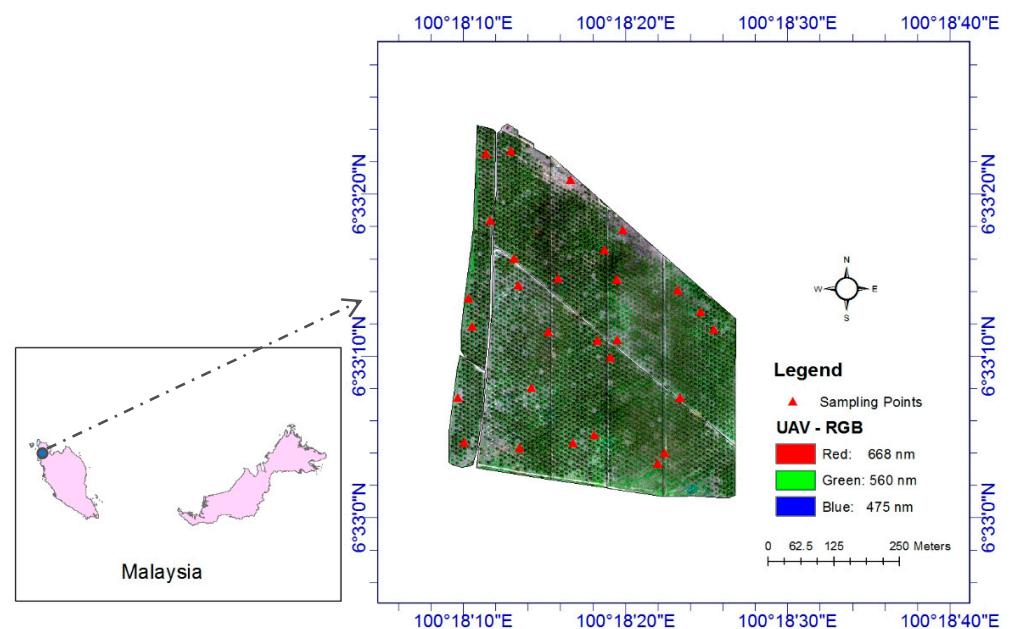


Figure 1. Oil palm cultivation area in Chuping, Perlis State, Malaysia.

In addition to the PALSAR-2 images, a DJI Phantom 4 Unmanned Aerial Vehicle (UAV), equipped with a Micasense[®] RedEdge camera (Micasense Inc., Seattle, WA, USA) multispectral sensor was employed to survey the study area on 17 January 2019. The Micasense[®] camera gathers information in five spectral bands, spanning the visible through red-edge and infrared spectrums. Specifically, red, green, blue, near-infrared, and red-edge images were captured at central wavelengths of 668, 560, 475, 840, and 717 nm, respectively. The sensor was calibrated on-site, prior to flight, using the reference panel for accurate ground reflectance calibration. The imagery from the UAV platform enabled us to compute the NDVI [66], as shown in Equation (3), in order to identify bare soil with NDVI values of less than 0.2. To confirm the classification was indeed bare soil, ground-truthing was performed.

$$NDVI = \frac{\rho_{840} - \rho_{668}}{\rho_{840} + \rho_{668}} \quad (3)$$

3. Methodology

The WCM was first developed by Attema and Ulaby [45] for alfalfa, corn, and wheat crops. It is a broadly applied model for vegetation-covered areas, because it is composed

of two components: the direct contribution of vegetation and the attenuation component. Many studies have successfully applied the WCM to various crops, such as winter wheat [55], wheat and corn [50], multi-crop agriculture [54], and forests [67]. The WCM was established on the assumption that the canopy's "cloud" was composed of similar water droplets, scattered randomly throughout the canopy [68]. In this study, the WCM was used to retrieve soil moisture data from oil palm crop using PALSAR-2 data. Based on the assumption that the influence of soil surface roughness on observed backscatter is consistent over a short timespan at a given site, the temporal variation in SAR backscattering will be solely a reflection of changes in vegetation and soil moisture [54]. Consequently, in this study, a multi-temporal SAR data set was used in the WCM. With the input of SAR-derived indices and field-gathered vegetation descriptors (from the LAI), it was possible to compare both the vegetation descriptors to evaluate the WCM and retrieve the soil moisture parameter.

The WCM considered both soil moisture and vegetation characteristics, with Equation (4) showing the four empirical coefficients: A and B are vegetative characteristics and C and D are soil parameters [69]. In Equations (5) and (6), parameter A corresponds to the albedo of the vegetation, with B being an attenuation factor. Parameter D indicates the sensitivity of the radar signal to soil moisture, while C can be a calibration constant in Equation (7). Equation (5) shows the backscatter coefficient from the direct contribution of vegetation, whereas Equation (6) gives the attenuation component for the vegetation-covered surface. Hence, the equation is modified to:

$$\sigma_{tot}^0 = \sigma_{veg}^0 + \tau^2 \sigma_{soil}^0 \quad (4)$$

where

$$\sigma_{veg}^0 = A \times V_1 \times \cos \theta \left(1 - \tau^2\right) \quad (5)$$

$$\tau^2 = \text{Exp} \left(-2 \times B \times V_2 \times \sec \theta\right) \quad (6)$$

$$\sigma_{soil}^0 = CM_v + D \quad (7)$$

The moisture content held in the canopy and its geometry have an impact on the backscatter coefficient in terms of both V_1 and V_2 . The soil moisture (M_v) is described in m^3/m^3 and θ represents the incidence angle of the SAR images. After solving for parameters C and D using a linear model fitting procedure, the values of C and D are replaced in Equations (5) and (6), allowing for the solution of parameters A and B using the nonlinear least squares method (NLSM) [51,53]. It has been reported that A and B can be estimated using Levenberg–Marquardt optimization in the NLSM [47]. However, descriptors relating to vegetation have varied implications for the WCM. Several experiments have been conducted, employing plant height, the LAI, the leaf–water area index (LWAI), and the normalized plant-water content (NPWC) as variables, to measure V_1 and V_2 [29,70,71]. In this study, the vegetation descriptors $V_1 = 1$ and $V_2 = \text{LAI}$ were chosen because they have contributed to the best model performance using other field-based descriptors such as LWAI and NPWC [61]. This is referred to as Model 1 (see Table 2). The SAR-derived indices were used for modeling the oil palm WCM and are referred to as Models 2, 3, and 4. The RVI, being derived from dual polarization [72], was used as shown in Equation (8). The RVI equation was initially introduced by proposing the use of the four polarizations (i.e., HH, HV, VH, and VV) [73]. However, it has been found that the RVI provides a good approximation of surface scattering when only two polarizations are used [74].

$$\text{RVI} = \frac{4\sigma_{HV}^0}{\sigma_{HH}^0 + \sigma_{HV}^0} \quad (8)$$

It has been noted that RVI values range from 0 to 1, with 0 being associated with bare soil and 1 with higher vegetation [75]. In this study, along with the RVI, other vegetation

descriptors, such as the calculated ratios $R_{HH/HV} = \frac{\sigma_{HH}^0}{\sigma_{HV}^0}$ and HV/HH as $R_{HV/HH} = \frac{\sigma_{HV}^0}{\sigma_{HH}^0}$, were used to evaluate the soil moisture (Table 2).

Table 2. Simplified WCM using modeled vegetation descriptors.

Model	Vegetation Descriptors, V_1 and V_2
1	$V_1 = 1, V_2 = LAI$
2	$V_1 = V_2 = RVI$
3	$V_1 = V_2 = R_{HH/HV}$
4	$V_1 = V_2 = R_{HV/HH}$

To evaluate the WCM for soil moisture data retrieval using the models listed in Table 2, the leave-one-out cross-validation (LOOCV) method was used—a deterministic validation procedure that enables accurate replication using the same data set [76]. Each time the model was evaluated, one of the data samples was omitted, with the remaining $n - 1$ data sample being used to train the model. The LOOCV method has been demonstrated as being superior to split-sample validation, especially when sample sizes are limited [77]. Model evaluation can be expressed in performance metrics, such as the coefficient of determination (R^2) and the root mean square error (RMSE) [78,79], calculated as shown in Equations (9) and (10), respectively. For each parameter combination, a pair of predicted and observed values were obtained.

$$R^2 = \left(\frac{\sum_{i=1}^n (X_{obs} - \overline{X_{obs}}) (X_{sim} - \overline{X_{sim}})}{\sqrt{\sum_{i=1}^n (X_{obs} - \overline{X_{obs}})^2 \sum_{i=1}^n (X_{sim} - \overline{X_{sim}})^2}} \right)^2 \quad (9)$$

$$RMSE = \sqrt{\frac{\sum_{i=1}^n (X_{sim} - X_{obs})^2}{n}} \quad (10)$$

The RMSE was estimated using Equation (9), where X_{sim} is the simulated σ_{tot}^0 and X_{obs} is the observed σ_{tot}^0 . The RMSE is widely accepted for assessing the gap between model predictions and actual observations from the environment in soil moisture-related studies [80,81]. Most scholars accept the RMSE for soil moisture data retrieval by referring to the Global Monitoring for Environment and Security (GMES) requirement from the European Space Agency for accuracy, with soil moisture values below $0.05 \text{ m}^3/\text{m}^3$ being considered as favoring the guidelines [82,83].

4. Results

4.1. WCM Parameterization

In the WCM approach, vegetation parameters describe the scattering from the vegetation cover on the ground. Estimation of the WCM parameters first requires calibration of the values for bare soil in order to obtain the soil-related parameters C and D from Equation (7), then correcting for the effects of vegetation on the backscattering coefficients. For parameters C and D, the input of field or SAR-based indicators, along with the incident angle and soil moisture, are required in order for the total backscatter to be calibrated. The WCM was calibrated differently for each model, for both σ_{HH}^0 and σ_{HV}^0 , in order to localize the vegetation parameters as shown in Table 3 using the LOOCV approach for cross-validation. The WCM parameterization is important for obtaining a good fit with the field measurements, as described in Equations (4)–(7), enabling the retrieval of the soil moisture values. Using the LOOCV method to estimate the actual error in the developed model, all the steps in the algorithm, including parameter tuning, have to be repeated in each cross-validation loop [83]. For the SAR-based vegetation descriptors, the RVI was derived from the PALSAR-2 images, where it has been shown to describe the structural vegetation characteristics, and the RVI correlates with the vegetation water content and

LAI indicators [84]. The $R_{HH/HV}$ and $R_{HV/HH}$ were employed to evaluate the potential use of these simple ratios as vegetation descriptors because the latter has been reported as being able to distinguish fluctuations in soil moisture using SAR data, and also to identify areas where the influence of soil surface roughness can be mitigated [58]. To evaluate the model further, a comparison of the WCM-modeled backscatter coefficients was checked against the observed backscatter coefficients using the respective polarization, as indicated in Section 4.2.

Table 3. Fitting of the WCM using HH and HV polarization.

Vegetation Descriptor by Model		Model Coefficients									
		HH					HV				
V_1	V_2	A	B	C	D	n	A	B	C	D	n
1	LAI	0.012	0.001	−26.015	−2.864	96	0.317	0.013	22.207	−23.866	96
RVI	RVI	0.319	0.017	−13.648	−5.784	96	0.613	0.008	24.556	−23.894	96
$R_{HH/HV}$	$R_{HH/HV}$	0.181	0.016	−11.663	−6.462	96	0.450	0.133	21.874	−22.487	96
$R_{HV/HH}$	$R_{HV/HH}$	0.758	0.007	−15.200	−5.900	96	0.826	0.010	20.320	−23.500	96

4.2. Sensitivity Backscatter Coefficient vs. Vegetation Descriptors

To understand the suitability of vegetation descriptors in the retrieval of soil moisture data over oil palm crops, four WCMs were used to evaluate the potential use of SAR-based parameters. SAR backscatter coefficients are connected to vegetation features on the ground, such as crop form, height, size, geometric arrangement, and density, all of which vary per crop [85,86]. In this study, a simplified WCM was evaluated in terms of both σ_{HH}^0 and σ_{HV}^0 to understand its polarization sensitivity to the oil palm crop. The results were determined using the model metrics of R^2 and the RMSE between the observed and WCM-simulated backscatter coefficients as shown in Table 4. Overall, using the LOOCV method, R^2 ranged from 0.930 to 0.983 for the HH polarization and from 0.948 to 0.991 for the HV, with the RMSE being 0.425–2.257 dB and 0.635–1.282 dB, respectively. Using the LAI field vegetation descriptor for the palms produced, a low RMSE value of 0.635 dB under HV polarization with $R^2 = 0.983$ (Table 4, Figure 2). For the RVI, the SAR-derived descriptor $R_{HH/HV}$ and $R_{HV/HH}$ were evaluated for the same day as the LAI indicator using Equation (1). Under the same polarization, when the RVI was used in the WCM, the model showed a higher RMSE of 0.702 dB with an R^2 of 0.975 recorded. The modeled backscatter coefficient for the vegetation descriptor $R_{HH/HV}$ (Model 3, Table 4) had an R^2 of 0.982 and an RMSE of 0.828 dB. For $R_{HV/HH}$, the RMSE was higher than for $R_{HH/HV}$, at 1.282 dB for σ_{HV}^0 , with an $R^2 = 0.930$.

Table 4. RSME values for the WCM-simulated and observed backscatter using PALSAR-2 with different vegetation descriptors.

Polarization	RMSE (dB)			
	Model 1	Model 2	Model 3	Model 4
HH	2.257	0.425	0.472	1.883
HV	0.635	0.702	0.828	1.282
Polarization	R^2			
	Model 1	Model 2	Model 3	Model 4
HH	0.948	0.990	0.991	0.964
HV	0.983	0.975	0.982	0.930

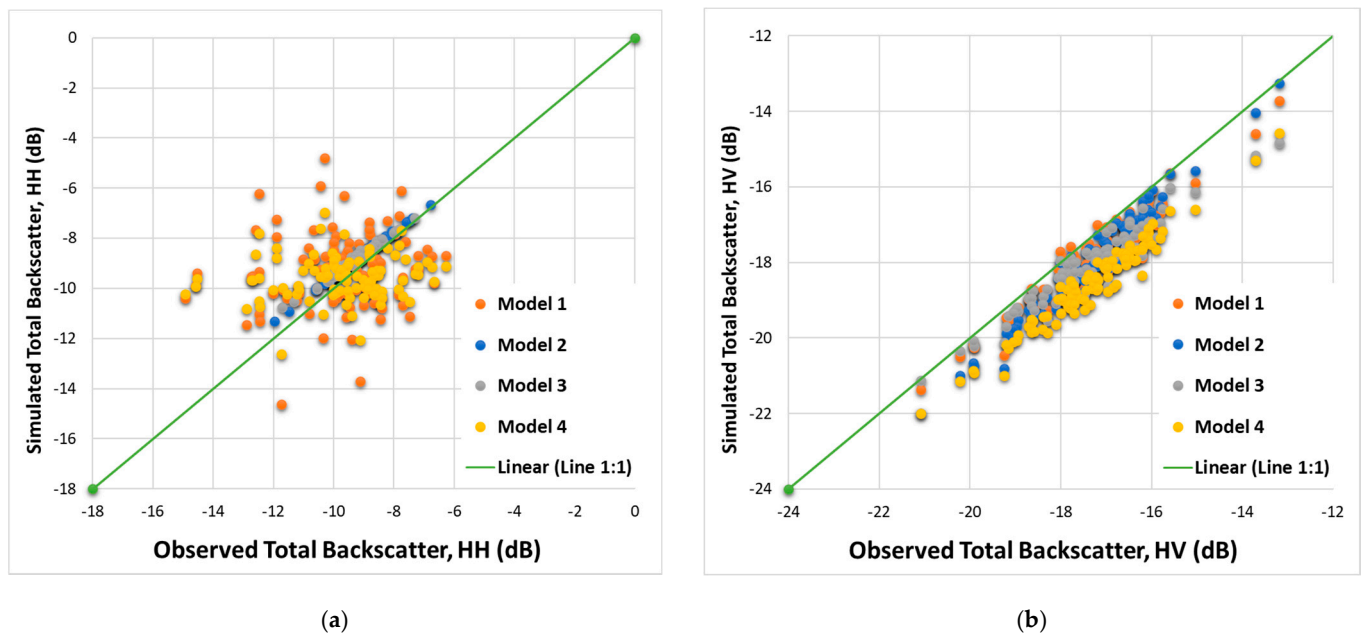


Figure 2. Scatterplots showing the simulated and observed backscatter coefficients under (a) HH and (b) HV polarization.

On the other hand, the HH polarization with the LAI vegetation descriptor had an R^2 of 0.948, with a higher RMSE, at 2.257 dB, than the HV polarization in the Model 1 (Table 4, Figure 2a). The Model 1 in HH polarization produced the highest RMSE values compared to the other models. In Model 3, the $R_{HH/HV}$, vegetation indicator was comparable with the RVI model with both being comparable to the LAI model under HH polarization. Both SAR-based model indicators showed a similar accuracy with RMSEs of 0.425 dB and 0.472 dB, respectively, as indicated in Table 4, and with an R^2 of 0.990 and 0.991. In the model using $R_{HV/HH}$, an R^2 value of 0.964 was observed with a higher RMSE of 1.883 dB.

4.3. Soil Moisture Data Retrieval

The purpose of this study was to retrieve soil moisture data from oil palm crops where soil moisture is an important indicator of the water requirements of the crop, being an important factor in crop development and yield [64,87]. Furthermore, the retrieval of soil moisture data is useful in seasonal or agricultural drought monitoring in terms of understanding the significant areas affected [28]. In this study, statistical metrics were employed in order to understand soil moisture data retrieval from the WCM used. Table 5 and Figure 3 show the data retrieval using Models 1–4 under HH and HV polarization. It was noted that, under both polarizations, the vegetation descriptors attempted to represent the vegetation layer as carefully as possible. Numerous studies have demonstrated that the type of vegetation, the geometric structure of its cover (including height, branch and leaf forms, and density distribution) and its water content have an effect on radar backscattering and radar wave transmittance in the plant canopy [88–90]. In order to minimize errors in the soil moisture content data, multiple angles, and multitemporal SAR data inversion were used to help to eradicate the consequences of the plant layer on the radar backscatter [90]. When the field-based LAI was used to retrieve the soil moisture data, the HV polarization showed a high R^2 of 0.949, with a low RMSE of 0.033 m^3/m^3 . Under HH polarization, however, the LAI indicator showed a higher RMSE of 0.087 m^3/m^3 .

Table 5. R^2 and the RMSEs for the soil moisture data retrieved and observed from an oil palm crops (in m^3/m^3) using PALSAR-2, given according to the proposed models.

Vegetation Descriptor by Model	Statistics Metrics			
	HH		HV	
	R^2	RMSE (m^3/m^3)	R^2	RMSE (m^3/m^3)
Model 1	0.901	0.087	0.949	0.033
Model 2	0.973	0.036	0.960	0.031
Model 3	0.946	0.049	0.974	0.049
Model 4	0.898	0.128	0.898	0.066

The main reason for evaluating the SAR-derived indicators was to avoid the cloud-cover concerns that arise from optical data, which mainly affects tropical regions [91]. From the SAR-derived Models 2–4 (Table 5), it was found that the HV polarization showed RMSEs ranging from 0.031 to 0.066 m^3/m^3 . This suggested that the HV polarization was consistent in retrieving the soil moisture data. This is similar to the mentioned descriptors, which showed a lower RMSE from the backscatter model fit (Table 4). This finding correlated with the field evaluation of the WCM, with the HV polarization providing a more accurate estimation of soil moisture [92]. The RVI produced the lowest RMSE among the other SAR-derived models at 0.031 m^3/m^3 . For the HH polarization, SAR-derived Models 2 and 3 had lower RMSE values of 0.036 and 0.049 m^3/m^3 , and with comparable R^2 values (Table 5). The SAR-derived indicators performed better than the field-based vegetation descriptor, according to Model 1, under HH polarization. However, the $R_{HV/HH}$ showed low accuracy in the RMSE comparison for both the polarizations, being 0.128 and 0.066 m^3/m^3 , respectively.

Our findings are in agreement with those of previous studies, in which it has been reported that RVI indicators in the WCM have been successfully evaluated to replace field indicators in order to overcome optical data concerns [41,62]. It was noted that the RVI model has been posited as a new descriptor that can be used to distinguish the backscattering from the crop canopy and the underlying soil surface in cases where the crop parameter cannot be obtained from the field, with the RVI being directly calculated from the SAR [55]. Overall, the soil moisture data retrieval in this study was successful, based on the parameterization of the WCM for the oil palm crop, with the use of the RVI and $R_{HH/HV}$ as vegetation descriptors proving as dependable as the LAI descriptors. However, the SAR-derived indicators were noted as producing lower RMSEs under HV polarization, similarly to the LAI descriptor under HV polarization. The scatterplots of the observed and retrieved soil moisture data, based on the polarization of each model, are shown in Figure 3.

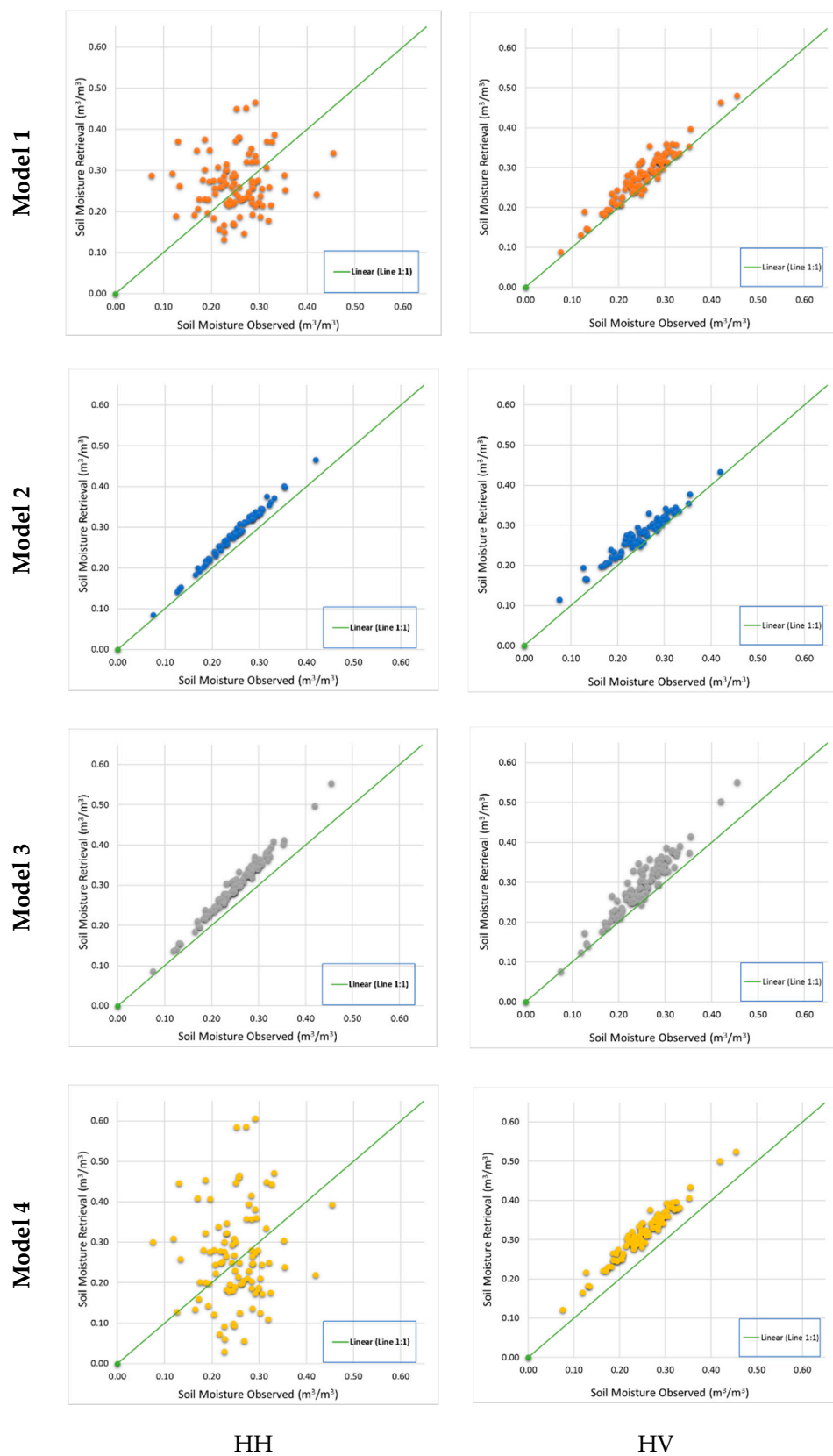


Figure 3. Scatterplots showing the observed and retrieved soil moisture data from an oil palm crop under both HH (left) and HV (right) polarization in different models in the L band.

5. Discussion

The WCM is a semi-empirical model, founded on theoretical ideas and relationships, but which employs a simplified method based on field- and SA-based parameters. In order to build the WCM, a calibration process was performed using variables, including LAI from the oil palm crop, soil moisture data from the field data collection as well as the backscattering coefficients, the RVI, $R_{HH/HV}$ and $R_{HV/HH}$, and the incidence angle from PALSAR-2. Using these variables, the parameters A, B, C, and D were considered in fine-tuning the WCM—important steps specific to each crop and location [49]. Adding on, to improve the fine-tuning estimation of the parameters mentioned, LOOCV was implemented using the concept of iteration. This fine-tuning of the parameters (Table 3) is dependent on the sensor configuration, vegetation cover and soil characteristics. In this instance, the terrain was relatively flat and, therefore, the oil palm backscattering contributed to the radar signal as shown in Figure 2. It is important to note that the vegetation parameters $V_1 = 1$ and $V_2 = \text{LAI}$ were used for comparison to the ground vegetation cover in this study, as these have previously been found to be the best soil moisture indicators, among other vegetation parameters, such as the LWAI and NPWC, for oil palm crop [61]. The results were in agreement with those of previous studies on other crops, with the LAI variable being superior in sugarcane, cherry, rice [46], and wheat [93]. The accuracy obtained in the retrieval of soil moisture data using the LAI (Table 5) showed that the HV polarization RMSE of $0.033 \text{ m}^3/\text{m}^3$ using the L band fulfilled the GMES requirement of $\text{RMSE} < 0.05 \text{ m}^3/\text{m}^3$. By contrast, the HH polarization produced a higher RMSE in this study than in another study that used PALSAR-2, where the soil moisture was variable, giving a retrieval accuracy of approximately 6.0% [94]. In relation to this, the HV polarization in the L band is more sensitive to the vegetation structure and biomass of oil palm when compared to HH polarization in peninsular Malaysia [95]. However, comparable results were found under VV polarization using the LAI in wheat, with an RMSE of 4.19% using the advanced SAR (ASAR) C-band sensor. For oil palm crop, using LAI in the field is a destructive, manual method [96], but it is widely regarded as the most accurate method for estimating the true LAI [97]. However, estimating LAI using this direct method is time-consuming, tedious, and labor-intensive [63].

L-band backscatter interacts at the top of the canopy as well as at the soil. Using this capability, the L-band SAR-derived descriptors were considered worthy of evaluation in order to obtain an understanding of the possibility of reducing this field-based variable into the WCM to allow for simplified model fine-tuning and soil moisture data retrieval. Positive correlations were found between all SAR-based descriptors and soil moisture in oil palm under HH polarization using the RVI and $R_{HH/HV}$ ranging from 0.036 to $0.049 \text{ m}^3/\text{m}^3$ RMSE, followed by $R_{HV/HH}$ with a RMSE accuracy of $0.128 \text{ m}^3/\text{m}^3$. For the RVI, $R_{HH/HV}$ and $R_{HV/HH}$ were employed where greater accuracy was found under the HV polarization than the HH polarization. Under HV polarization, the RVI vegetation descriptors used in multiple crops have demonstrated an accuracy of $0.085 \text{ m}^3/\text{m}^3$ [54], which was improved in this study at $0.031 \text{ m}^3/\text{m}^3$.

Similarly, using $R_{HH/VV}$, $R_{VH/VV}$, RVI, and the generalized volume scattering model based radar vegetation index, employed in a recent study, showed similar accuracies to the findings of this study [56]. In addition, WCM studies using optical-based descriptors (commonly the NDVI) have also been found to be accurate to within the GMES standards. In comparing the NDVI with $R_{VH/VV}$, crop phenology and crop growth changes have been demonstrated and found to have an accuracy of $0.12 \text{ cm}^3/\text{cm}^3$ in corn at the growth level [57]. It was noted that the accuracy of soil moisture data retrieval can be affected by the preprocessing and filtering process; hence, some consideration must be given to evaluating the filtering window size, incident angle, and the SAR imaging resolution. Soil moisture data retrieved from multi-polarized and multi-angled RADARSAT-2 images have produced WCMs with accuracies of $\text{RMSE} = 5.9\%$ and 6.6% , respectively [98]. Using the WCM, Zribi et al. [99] obtained comparable results for a semi-arid environment, at $\text{RMSE} = 0.06 \text{ m}^3/\text{m}^3$, using ASAR data. However, because crop structures vary in time and

space, and radar interactions between the soil and vegetation are complex, the proposed approach's spatial and temporal transferability requires more measurements of soil and vegetation properties, and corresponding radar observations, to provide more robust results. On the other hand, cross-validation in this study was achieved using the LOOCV method to enable fine-tuning of the parameters and error reduction in the evaluated data set.

Based on the outcome of this study, we envisage that the WCM approach can be embedded into crop automated irrigation systems, particularly in oil palm, where appropriate soil moisture must be accessible, since insufficient or excessive moisture will have a detrimental effect on nutrient uptake and yields. On the other hand, soil moisture retrieval from PALSAR-2 can reduce laborious soil sampling work and result in time and cost savings. Using the findings from this study, we were able to successfully reduce field-based parameters, allowing the WCM approach to be evaluated further to develop an efficient soil moisture model for the oil palm industry, particularly in rural plantation areas with limited physical access for conventional soil sampling.

6. Conclusions

In this study, the WCM model was calibrated using L band SAR data, with the field-based LAI indicator and SAR-derived RVI, $R_{HH/HV}$, and $R_{HV/HH}$ as input vegetation descriptors for an oil palm crop with in-field soil moisture. The aim was to evaluate the SAR-derived indicators from PALSAR-2 for their suitability in reducing the need for field-based parameter data collection. Our findings allow a simplification of the WCM that enables SAR benefits to be adapted for soil moisture data retrieval in oil palm. The model fit showed that with HV polarization, the RVI and $R_{HH/HV}$ produced a good replication backscatter coefficient compared to using the LAI as the vegetation parameter. The WCM modeled using the RVI and $R_{HH/HV}$ had accuracies of 0.425 and 0.472 dB RMSE. With HV polarization, the field-based LAI indicator showed the model fit with an R^2 of 0.983 and RMSE of 0.635 dB, using PALSAR-2 data. Our results showed that the soil moisture data retrieval was successful with an RMSE ranging as low as $0.033 \text{ m}^3/\text{m}^3$ using the field-based LAI indicator under HV polarization. The SAR-based RVI indicator, however, gave better accuracy with HV polarization at $0.031 \text{ m}^3/\text{m}^3$. The $R_{HH/HV}$ polarization demonstrated an equally good capability of soil moisture data retrieval, at an RMSE of $0.049 \text{ m}^3/\text{m}^3$ with the same polarization.

Based on these results, it was demonstrated that the WCM is applicable to oil palm crop, with the performance of the model being evaluated using different vegetation descriptors, providing an understanding of the potential use of SAR-derived vegetation descriptors using PALSAR-2. It is suggested that full polarization of the L band to be used for exploiting the SAR-based indicators in oil palm WCMs, and also to examine the impact of the VH and VV polarization effects. For future work, C band backscattering from the oil palm trees crown canopies can be more thoroughly evaluated to be implemented in the WCM for biophysical estimation of vegetation cover. Investigation of the C band, using field-based vegetation water content measurements in the oil palm canopy can be explored using Equation (6) to study the accuracy of retrieving vegetation variable, e.g., LAI.

Author Contributions: Conceptualization, V.S. and A.R.M.S.; data curation, V.S.; formal analysis, V.S. and A.R.M.S.; investigation, V.S., A.R.M.S. and A.W.; methodology, V.S., A.R.M.S., A.W., M.R.K., Y.P.L. and W.T.; resources, A.R.M.S., A.W., M.R.K., Y.P.L. and W.T.; software, V.S. and M.R.K.; supervision, A.R.M.S., A.W., M.R.K., Y.P.L. and W.T.; validation, V.S., A.R.M.S., A.W., M.R.K., Y.P.L. and W.T.; visualization, A.R.M.S. and A.W.; writing—original draft, V.S., A.R.M.S., and Y.P.L.; writing—review and editing, V.S., A.R.M.S., A.W., M.R.K., Y.P.L. and W.T. All authors have read and agreed to the published version of the manuscript.

Funding: The PALSAR-2 data were gathered with funding from the Japanese Aerospace Agency as part of the Earth Observation Research Announcement 2 partnership (Principal Investigator No. ER2A2N180).

Institutional Review Board Statement: Not applicable.

Informed Consent Statement: Not applicable.

Data Availability Statement: The PALSAR-2 data obtained are subject to restrictions, as a special request for high-resolution data has to be made.

Acknowledgments: The authors would like to express their gratitude to Rajah Selvarajah for providing financial support for the acquisition of the UAV data and for the fieldwork logistics necessary to finish the research. The authors thank the Soil and Water Conservation Laboratory, Department of Biological and Agricultural Engineering, Faculty of Engineering, Universiti Putra Malaysia (UPM), and especially Mohamad Hafis bin Ramli, for providing the equipment to extract the soil samples and the oven for drying them. All authors are grateful to Ghazali bin Kassim for arranging for us to borrow the GPS equipment used for locating the soil samples in the field from the Spatial Information System Laboratory, Biological and Agricultural Engineering, Faculty of Engineering, UPM. FGV R&D Sdn Bhd are thanked for facilitating the collection of data in the field, particularly Mohd Shahkhirat bin Norizan, Syahidah Abu Hassan, Muhamad Mazuan Bin Yahaya, Haryati Abidin, Noorsusilawati bt. Mandangan, Mohd Mahfuz Roslan, Muhammad Farid Abdul Rahim, and Mohd Na'aim bin Samad.

Conflicts of Interest: The authors declare no conflict of interest.

References

1. Quezada, J.C.; Etter, A.; Ghazoul, J.; Buttler, A.; Guillaume, T. Carbon neutral expansion of oil palm plantations in the Neotropics. *Sci. Adv.* **2019**, *5*, eaaw4418. [[CrossRef](#)] [[PubMed](#)]
2. Alam, A.S.A.F.; Er, A.C.; Begum, H. Malaysian oil palm industry: Prospect and problem. *J. Food Agric. Environ.* **2015**, *13*, 143–148.
3. Arunachalam, V. Oil Palm. In *Genomics of Cultivated Palms*, 1st ed.; Elsevier Inc Publications: Amsterdam, The Netherlands, 2012; pp. 29–48.
4. Voora, V.; Larrea, C.; Bermúdez, S.; Baliño, S. *Global Market Report: Palm Oil*; International Institute for Sustainable Development: Winnipeg, MB, Canada, 2020.
5. Lim, C.H.; Cheah, Z.H.; Lee, X.H.; How, B.S.; Ng, W.P.Q.; Ngan, S.L.; Lim, S.; Lam, H.L. Harvesting and evacuation route optimisation model for fresh fruit bunch in the oil palm plantation site. *J. Clean. Prod.* **2021**, *307*, 127238. [[CrossRef](#)]
6. Suharjito; Elwirehardja, G.N.; Prayoga, J.S. Oil palm fresh fruit bunch ripeness classification on mobile devices using deep learning approaches. *Comput. Electron. Agric.* **2021**, *188*, 106359. [[CrossRef](#)]
7. Jaroenkietkajorn, U.; Gheewala, S.H. Land suitability assessment for oil palm plantations in Thailand. *Sustain. Prod. Consum.* **2021**, *28*, 1104–1113. [[CrossRef](#)]
8. Bos, U.; Maier, S.D.; Horn, R.; Leistner, P.; Finkbeiner, M. A GIS based method to calculate regionalized land use characterization factors for life cycle impact assessment using LANCA[®]. *Int. J. Life Cycle Assess.* **2020**, *25*, 1259–1277. [[CrossRef](#)]
9. Sehler, R.; Li, J.; Reager, J.; Ye, H. Investigating Relationship Between Soil Moisture and Precipitation Globally Using Remote Sensing Observations. *J. Contemp. Water Res. Educ.* **2019**, *168*, 106–118. [[CrossRef](#)]
10. Li, J.; Sehler, R.; Reager, J.T., II; Ye, H. Using Satellite-based Observations to Investigate the Soil Moisture—Precipitation Relationship. *AGU Fall Meet. Abstr.* **2019**, *2019*, 1910.
11. Ali, G. Climate change and associated spatial heterogeneity of Pakistan: Empirical evidence using multidisciplinary approach. *Sci. Total Environ.* **2018**, *634*, 95–108. [[CrossRef](#)] [[PubMed](#)]
12. Fowler, H.J.; Blenkinsop, S.; Tebaldi, C. Linking climate change modelling to impacts studies: Recent advances in downscaling techniques for hydrological modelling. *Int. J. Clim.* **2007**, *27*, 1547–1578. [[CrossRef](#)]
13. Shukla, A.; Panchal, H.; Mishra, D.M.; Patel, P.R.; Srivastava, H.S.; Patel, P. Soil Moisture Estimation using Gravimetric Technique and FDR Probe Technique: A Comparative Analysis. *Am. Int. J. Res. Form. Appl. Nat. Sci.* **2014**, *8*, 89–92.
14. Degirmenci, H.; Gonen, E.; Boyaci, S.; Resources, W.; Location, T. A comparison of the gravimetric and TDR methods in terms of determining the soil water content of the corn plant. *Sci. Pap.-Ser. A-Agron.* **2016**, *59*, 153–158.
15. Teixeira, W.G.; Huwe, B.; Schroth, G.; Marques, J.D. Sampling and TDR probe insertion in the determination of the volumetric soil water content. *Rev. Bras. Ciênc. Solo* **2003**, *27*, 575–582. [[CrossRef](#)]
16. Kaleita, A.L.; Tian, L.F.; Hirschi, M.C. Relationship between Soil Moisture Content and Soil Surface Reflectance. *Trans. ASAE* **2005**, *48*, 1979–1986. [[CrossRef](#)]
17. Al-Mamoori, S.K.; Al-Maliki, L.A.; Al-Sulttani, A.H.; El-Tawil, K.; Al-Ansari, N. Statistical analysis of the best GIS interpolation method for bearing capacity estimation in An-Najaf City, Iraq. *Environ. Earth Sci.* **2021**, *80*, 683. [[CrossRef](#)]
18. Chen, H.; Fan, L.; Wu, W.; Liu, H.-B. Comparison of spatial interpolation methods for soil moisture and its application for monitoring drought. *Environ. Monit. Assess.* **2017**, *189*, 525. [[CrossRef](#)]
19. Gilewski, P. Impact of the Grid Resolution and Deterministic Interpolation of Precipitation on Rainfall-Runoff Modeling in a Sparsely Gauged Mountainous Catchment. *Water* **2021**, *13*, 230. [[CrossRef](#)]

20. İmamoğlu, M.Z.; Sertel, E. Analysis of Different Interpolation Methods for Soil Moisture Mapping Using Field Measurements and Remotely Sensed Data. *Int. J. Environ. Geoinformatics* **2016**, *3*, 11–25. [CrossRef]
21. Oliver, M.A.; Webster, R. Geostatistical Prediction: Kriging. In *Basic Steps in Geostatistics: The Variogram and Kriging*; Springer Nature: Basingstoke, UK, 2015; pp. 43–69. [CrossRef]
22. Shen, Q.; Wang, Y.; Wang, X.; Liu, X.; Zhang, X.; Zhang, S. Comparing interpolation methods to predict soil total phosphorus in the Mollisol area of Northeast China. *CATENA* **2019**, *174*, 59–72. [CrossRef]
23. Guo, X.; Fu, Q.; Hang, Y.; Lu, H.; Gao, F.; Si, J. Spatial variability of soil moisture in relation to land use types and topographic features on hillslopes in the black soil (mollisols) area of northeast China. *Sustainability* **2020**, *12*, 3552. [CrossRef]
24. Degré, A.; Ly, S.; Charles, C. Different methods for spatial interpolation of rainfall data for operational hydrology and hydrological modeling at watershed scale: A review. *Biotechnol. Agron. Société Environ.* **2013**, *17*, 392–406. Available online: <https://popups.uliege.be/1780-4507> (accessed on 11 October 2021).
25. Yarak, K.; Witayangkurn, A.; Kritiyutanont, K.; Arunplod, C.; Shibasaki, R. Oil palm tree detection and health classification on high-resolution imagery using deep learning. *Agriculture* **2021**, *11*, 183. [CrossRef]
26. Malinee, R.; Stratoulis, D.; Nuthammachot, N. Detection of oil palm disease in plantations in krabi province, thailand with high spatial resolution satellite imagery. *Agriculture* **2021**, *11*, 251. [CrossRef]
27. Ibrahim, A.L.; Hashim, M.; Ali, M.I.; Rasib, W.; Kadir, W.H.W.; Sumari, M.R.; Haron, K. Detecting and Mapping Nutrients Concentration in Oil Palm Plantation Using Remote Sensing and Geographic Information System. In Proceedings of the PIPOC 2003 International Palm Oil Congress (Agriculture), Kuala Lumpur, Malaysia, 24–28 August 2003; pp. 261–271.
28. Zhu, L.; Suomalainen, J.; Liu, J.; Hyyppä, J.; Kaartinen, H.; Haggren, H. A Review: Remote Sensing Sensors. Available online: <https://books.google.co.jp/books?id=8m6QDwAAQBAJ&printsec=frontcover&hl=zh-CN#v=onepage&q&f=false> (accessed on 3 November 2021).
29. Xue, J.; Su, B. Significant Remote Sensing Vegetation Indices: A Review of Developments and Applications. *J. Sens.* **2017**, *2017*, 1353691. [CrossRef]
30. Shashikant, V.; Shariff, A.R.M.; Nordin, L.; Pradhan, B. NDVI of Oil Palm Trees by Landsat-5 Imagery. In Proceedings of the 33rd Conference on Remote Sensing, Pattaya, Thailand, 26–30 November 2012; p. 5.
31. Lehmann, E.A.; Caccetta, P.; Lowell, K.; Mitchell, A.; Zhou, Z.-S.; Held, A.; Milne, T.; Tapley, I. SAR and optical remote sensing: Assessment of complementarity and interoperability in the context of a large-scale operational forest monitoring system. *Remote Sens. Environ.* **2015**, *156*, 335–348. [CrossRef]
32. Saatchi, S.S. Application of SAR Remote Sensing in Land Surface Processes Over Tropical Region. In Proceedings of the Anais VIII Simposio Brasileiro de Sensoriamento Remoto, Salvador, Brasil, 14–19 April 1996; pp. 369–374.
33. Ottinger, M.; Kuenzer, C. Spaceborne L-Band Synthetic Aperture Radar Data for Geoscientific Analyses in Coastal Land Applications: A Review. *Remote Sens.* **2020**, *12*, 2228. [CrossRef]
34. Daliman, S.; Rahman, S.A.; Abu Bakar, S.; Busu, I. Segmentation of oil palm area based on GLCM-SVM and NDVI. In Proceedings of the 2014 IEEE REGION 10 SYMPOSIUM, Kuala Lumpur, Malaysia, 14–16 April 2014; pp. 645–650. [CrossRef]
35. Teng, K.C.; Koay, J.Y.; Tey, S.H.; Lim, K.S.; Ewe, H.T.; Chuah, H.T. A Dense Medium Microwave Backscattering Model for the Remote Sensing of Oil Palm. *IEEE Trans. Geosci. Remote Sens.* **2014**, *53*, 3250–3259. [CrossRef]
36. Ibharim, N.; Mustapha, M.; Lihan, T.; Mazlan, A. Mapping mangrove changes in the Matang Mangrove Forest using multi temporal satellite imageries. *Ocean Coast. Manag.* **2015**, *114*, 64–76. [CrossRef]
37. Woodhouse, I.H. *Introduction to Microwave Remote Sensing*; CRC Press: Boca Raton, FL, USA, 2017.
38. Li, L.; Dong, J.; Tenku, S.N.; Xiao, X. Mapping Oil Palm Plantations in Cameroon Using PALSAR 50-m Orthorectified Mosaic Images. *Remote Sens.* **2015**, *7*, 1206–1224. [CrossRef]
39. Dong, X.; Quegan, S.; Yumiko, U.; Hu, C.; Zeng, T. Feasibility Study of C- and L-band SAR Time Series Data in Tracking Indonesian Plantation and Natural Forest Cover Changes. *IEEE J. Sel. Top. Appl. Earth Obs. Remote Sens.* **2015**, *8*, 3692–3699. [CrossRef]
40. Fadaei, H.; Ishii, R.; Suzuki, R.; Kendawang, J.J. Detection of oil palm and acacia plantation areas using object based classification in sarawak, Malaysia. In Proceedings of the 34th Asian Conference on Remote Sensing (ACRS), Bali, Indonesia, 20–24 October 2013; pp. 1–7.
41. Hashim, I.; Shariff, A.; Bejo, S.; Muharam, F.; Ahmad, K. Machine-Learning Approach Using SAR Data for the Classification of Oil Palm Trees That Are Non-Infected and Infected with the Basal Stem Rot Disease. *Agronomy* **2021**, *11*, 532. [CrossRef]
42. Reiche, J.; Lucas, R.; Mitchell, A.L.; Verbesselt, J.; Hoekman, D.H.; Haarpaintner, J.; Kellndorfer, J.M.; Rosenqvist, A.; Lehmann, E.A.; Woodcock, C.E.; et al. Combining satellite data for better tropical forest monitoring. *Nat. Clim. Chang.* **2016**, *6*, 120–122. [CrossRef]
43. Kumar, P.; Prasad, R.; Choudhary, A.; Gupta, D.K.; Mishra, V.N.; Vishwakarma, A.K.; Singh, A.K.; Srivastava, P.K. Comprehensive evaluation of soil moisture retrieval models under different crop cover types using C-band synthetic aperture radar data. *Geocarto Int.* **2018**, *34*, 1022–1041. [CrossRef]
44. Petropoulos, G.P.; Ireland, G.; Barrett, B. Surface soil moisture retrievals from remote sensing: Current status, products & future trends. *Phys. Chem. Earth Parts A/B/C* **2015**, *83–84*, 36–56.
45. Attema, E.P.W.; Ulaby, F.T. Vegetation modeled as a water cloud. *Radio Sci.* **1978**, *13*, 357–364. [CrossRef]

46. Said, S.; Kothiyari, U.; Arora, M. Vegetation effects on soil moisture estimation from ERS-2 SAR images. *Hydrol. Sci. J.* **2012**, *57*, 517–534. [[CrossRef](#)]
47. Chauhan, S.; Srivastava, H.S.; Patel, P. Improved parameterization of water cloud model for hybrid-polarized backscatter simulation using interaction factor. *ISPRS—Int. Arch. Photogramm. Remote Sens. Spat. Inf. Sci.* **2017**, *XLII-4/W2*, 61–66. [[CrossRef](#)]
48. Léonard, A.; Bériaux, E.; Defourny, P. Complementarity of linear polarizations in C-band SAR imagery to estimate leaf area index for maize and winter wheat. *ESA Living Planet Symp.* **2013**, *12*, 957–964.
49. Bériaux, E.; Lucau-Danila, C.; Auquier, E.; Defourny, P. Multiyear independent validation of the water cloud model for retrieving maize leaf area index from SAR time series. *Int. J. Remote Sens.* **2013**, *34*, 4156–4181. [[CrossRef](#)]
50. Zhang, L.; Meng, Q.; Yao, S.; Wang, Q.; Zeng, J.; Zhao, S.; Ma, J. Soil Moisture Retrieval from the Chinese GF-3 Satellite and Optical Data over Agricultural Fields. *Sensors* **2018**, *18*, 2675. [[CrossRef](#)]
51. Tao, L.; Wang, G.; Chen, X.; Li, J.; Cai, Q. Estimation of soil moisture using a vegetation scattering model in wheat fields. *J. Appl. Remote Sens.* **2019**, *13*, 044503. [[CrossRef](#)]
52. Park, S.-E.; Jung, Y.T.; Cho, J.-H.; Moon, H.; Han, S.-H. Theoretical Evaluation of Water Cloud Model Vegetation Parameters. *Remote Sens.* **2019**, *11*, 894. [[CrossRef](#)]
53. Khabazan, S.; Hosseini, M.; Saradjian, M.R.; Motagh, M.; Magagi, R. Accuracy Assessment of IWCM Soil Moisture Estimation Model in Different Frequency and Polarization Bands. *J. Indian Soc. Remote Sens.* **2015**, *43*, 859–865. [[CrossRef](#)]
54. Li, J.; Wang, S. Using SAR-Derived Vegetation Descriptors in a Water Cloud Model to Improve Soil Moisture Retrieval. *Remote Sens.* **2018**, *10*, 1370. [[CrossRef](#)]
55. Yue, J.; Yang, G.; Qi, X.; Wang, Y. Soil moisture retrieval in well covered farmland by Radarsat-2 SAR data. *Int. Geosci. Remote Sens. Symp.* **2016**, 1699–1702. [[CrossRef](#)]
56. Bhogapurapu, N.; Mandal, D.; Rao, Y.S.; Bhattacharya, A. Soil Moisture Retrieval Using SAR Derived Vegetation Descriptors in Water Cloud Model. In Proceedings of the IGARSS 2020—2020 IEEE International Geoscience and Remote Sensing Symposium, Waikoloa, HI, USA, 26 September–2 October 2020; pp. 4696–4699. [[CrossRef](#)]
57. Wang, Z.; Zhao, T.; Qiu, J.; Zhao, X.; Li, R.; Wang, S. Microwave-based vegetation descriptors in the parameterization of water cloud model at L-band for soil moisture retrieval over croplands. *GIScience Remote Sens.* **2020**, *58*, 48–67. [[CrossRef](#)]
58. Jacome, A.; Bernier, M.; Chokmani, K.; Gauthier, Y.; Poulin, J.; De Sève, D. Monitoring Volumetric Surface Soil Moisture Content at the La Grande Basin Boreal Wetland by Radar Multi Polarization Data. *Remote Sens.* **2013**, *5*, 4919–4941. [[CrossRef](#)]
59. Baronti, S.; del Frate, F.; Ferrazzoli, P.; Paloscia, S.; Pampaloni, P.; Schiavon, G. Sar Polarimetric features of agricultural areas. *Int. J. Remote Sens.* **2010**, *16*, 2639–2656. [[CrossRef](#)]
60. Shashikant, V.; Shariff, A.M.; Wayayok, A.; Kamal, R.; Lee, Y.; Takeuchi, W. Utilizing TVDI and NDWI to Classify Severity of Agricultural Drought in Chuping, Malaysia. *Agronomy* **2021**, *11*, 1243. [[CrossRef](#)]
61. Shashikant, V.; Shariff, A.R.M.; Wayayok, A.; Kamal, R.; Lee, Y.P.; Takeuchi, W. Vegetation Effects on Soil Moisture Retrieval from Water Cloud Model Using PALSAR-2 for Oil Palm Trees. *Remote Sens.* **2021**, *13*, 4023. [[CrossRef](#)]
62. Kok, Z.H.; Shariff, A.R.B.M.; Khairunniza-Bejo, S.; Kim, H.-T.; Ahamed, T.; Cheah, S.S.; Wahid, S.A.A. Plot-Based Classification of Macronutrient Levels in Oil Palm Trees with Landsat-8 Images and Machine Learning. *Remote Sens.* **2021**, *13*, 2029. [[CrossRef](#)]
63. Awal, M.A.; Wan Ishak, W.I. Measurement of Oil Palm LAI by Manual and LAI-2000 Method. *Asian J. Sci. Res.* **2007**, *1*, 49–56. [[CrossRef](#)]
64. Motohka, T.; Isoguchi, O.; Sakashita, M.; Shimada, M. ALOS-2 PALSAR-2 Cal/Val Updates. In Proceedings of the JAXA/EORC Joint PI Meeting of Global Environment Observation Mission FY2017, Tokyo, Japan, 22–26 January 2018.
65. Ozdarici, A.; Conference, Z.A. A comparison of SAR filtering techniques on agricultural area identification. In Proceedings of the Imaging and Geospatial Information Society (ASPRS), San Diego, CA, USA, 26–30 April 2010.
66. Tucker, C.J. Red and photographic infrared linear combinations for monitoring vegetation. *Remote Sens. Environ.* **1979**, *8*, 127–150. [[CrossRef](#)]
67. Pulliainen, J.T.; Heiska, K.; Hyyppä, J.; Hallikainen, M.T. Backscattering Properties of Boreal Forests at the C and X-Bands. *IEEE Trans. Geosci. Remote Sens.* **1994**, *32*, 1041–1050. [[CrossRef](#)]
68. Ulaby, F.; Allen, C.; Eger, G.; Kanemasu, E. Relating the microwave backscattering coefficient to leaf area index. *Remote Sens. Environ.* **1984**, *14*, 113–133. [[CrossRef](#)]
69. Prévot, L.; Champion, I.; Guyot, G. Estimating surface soil moisture and leaf area index of a wheat canopy using a dual-frequency (C and X bands) scatterometer. *Remote Sens. Environ.* **1993**, *46*, 331–339. [[CrossRef](#)]
70. Xu, H.; Steven, M.D.; Jaggard, K.W. Monitoring leaf area of sugar beet using ERS-1 SAR data. *Int. J. Remote Sens.* **1996**, *17*, 3401–3410. [[CrossRef](#)]
71. Dabrowska-Zielinska, K.; Inoue, Y.; Kowalik, W.; Gruszczynska, M. Inferring the effect of plant and soil variables on C- and L-band SAR backscatter over agricultural fields, based on model analysis. *Adv. Space Res.* **2007**, *39*, 139–148. [[CrossRef](#)]
72. Charbonneau, F.; Trudel, M.; Fernandes, R. Use of Dual Polarization and Multi-Incidence SAR for soil permeability mapping. In Proceedings of the 2005 Advanced Synthetic Aperture Radar (ASAR) Workshop, St-Hubert, QC, Canada, 15–17 November 2005.
73. Kim, Y.; Van Zyl, J.J. A Time-Series Approach to Estimate Soil Moisture Using Polarimetric Radar Data. *IEEE Trans. Geosci. Remote Sens.* **2009**, *47*, 2519–2527. [[CrossRef](#)]
74. Trudel, M.; Charbonneau, F.; Leconte, R. Using RADARSAT-2 polarimetric and ENVISAT-ASAR dual-polarization data for estimating soil moisture over agricultural fields. *Can. J. Remote Sens.* **2012**, *38*, 514–527.

75. Kim, Y.-H.; Oh, J. Comparative Analysis of the Multispectral Vegetation Indices and the Radar Vegetation Index. *J. Korean Soc. Surv. Geodesy, Photogramm. Cartogr.* **2014**, *32*, 607–615. [[CrossRef](#)]
76. Akhtar, A.M.; Qazi, W.A.; Ahmad, S.R.; Gilani, H.; Mahmood, S.A.; Rasool, A. Integration of high-resolution optical and SAR satellite remote sensing datasets for aboveground biomass estimation in subtropical pine forest, Pakistan. *Environ. Monit. Assess.* **2020**, *192*, 584. [[CrossRef](#)] [[PubMed](#)]
77. Schönbrodt-Stitt, S.; Ahmadian, N.; Kurtenbach, M.; Conrad, C.; Romano, N.; Bogen, H.R.; Vereecken, H.; Nasta, P. Statistical Exploration of SENTINEL-1 Data, Terrain Parameters, and in-situ Data for Estimating the Near-Surface Soil Moisture in a Mediterranean Agroecosystem. *Front. Water* **2021**, *3*, 75. [[CrossRef](#)]
78. Wang, H.; Allain-Bailhache, S.; Méric, S.; Pottier, É.; Allain, S.; Pottier, E. Soil Parameter Retrievals Over Bare Agricultural Fields Using Multi-angular RADARSAT-2 Dataset. *IEEE J. Sel. Top. Appl. Earth Obs. Remote Sens.* **2016**, *9*, 5666–5676. [[CrossRef](#)]
79. Han, D.; Wang, P.; Tansey, K.; Zhou, X.; Zhang, S.; Tian, H.; Zhang, J.; Li, H. Linking an agro-meteorological model and a water cloud model for estimating soil water content over wheat fields. *Comput. Electron. Agric.* **2020**, *179*, 105833. [[CrossRef](#)]
80. Li, Y.; Zhang, C.; Heng, W. Retrieving Surface Soil Moisture over Wheat-Covered Areas Using Data from Sentinel-1 and Sentinel-2. *Water* **2021**, *13*, 1981. [[CrossRef](#)]
81. Paloscia, S.; Pettinato, S.; Santi, E.; Notarnicola, C.; Pasolli, L.; Reppucci, A. Soil moisture mapping using Sentinel-1 images: Algorithm and preliminary validation. *Remote Sens. Environ.* **2013**, *134*, 234–248. [[CrossRef](#)]
82. Santi, E.; Paloscia, S.; Pettinato, S.; Notarnicola, C.; Pasolli, L.; Pistocchi, A. Remote Sensing Comparison between SAR Soil Moisture Estimates and Hydrological Model Simulations over the Scriveria Test Site. *Remote Sens.* **2013**, *5*, 4961–4976. [[CrossRef](#)]
83. Varma, S.; Simon, R. Bias in error estimation when using cross-validation for model selection. *BMC Bioinform.* **2006**, *7*, 91. [[CrossRef](#)]
84. Kim, Y.; Jackson, T.; Bindlish, R.; Lee, H.; Hong, S. Radar Vegetation Index for Estimating the Vegetation Water Content of Rice and Soybean. *IEEE Geosci. Remote Sens. Lett.* **2011**, *9*, 564–568. [[CrossRef](#)]
85. Joshi, N.P.; Mitchard, E.T.A.; Schumacher, J.; Johannsen, V.K.; Saatchi, S.; Fensholt, R. L-Band SAR Backscatter Related to Forest Cover, Height and Aboveground Biomass at Multiple Spatial Scales across Denmark. *Remote Sens.* **2015**, *7*, 4442–4472. [[CrossRef](#)]
86. Goh, K.J.; Teo, C.B. Agronomic Principles and Practices of Fertilizer Management Of Oil Palm. *Agron. Princ. Pract. Oil Palm Cultiv.* **2011**, 241–389.
87. Disney, M.; Lewis, P.; Saich, P. 3D modelling of forest canopy structure for remote sensing simulations in the optical and microwave domains. *Remote Sens. Environ.* **2006**, *100*, 114–132. [[CrossRef](#)]
88. Pizaña, J.M.G.; Hernández, J.M.N.; Romero, N.C. Remote Sensing-Based Biomass Estimation. Available online: https://books.google.co.jp/books?hl=zh-CN&lr=&id=Wm-QDwAAQBAJ&oi=fnd&pg=PA3&dq=Remote+Sensing+Based+Biomass+Estimation.+Environ.+Appl.+Remote+Sens.+2016&ots=CkzgeLf5eT&sig=zPDDULDOZN6dR55GnHBQjxYY76M&redir_esc=y#v=onepage&q&f=false (accessed on 3 November 2021).
89. Ghasemi, N.; Sahebi, M.R.; Mohammadzadeh, A. A review on biomass estimation methods using synthetic aperture radar data. *Int. J. Ofgeomatics Geosci.* **2011**, *1*, 776–788.
90. Srivastava, H.S.; Patel, P.; Sharma, Y.; Navalgund, R.R. Large-Area Soil Moisture Estimation Using Multi-Incidence-Angle RADARSAT-1 SAR Data. *IEEE Trans. Geosci. Remote Sens.* **2009**, *47*, 2528–2535. [[CrossRef](#)]
91. Hoekman, D.; Quinones, M.; Vissers, M. K&C Science Report—Phase 1 Tropical Forest and Wetlands Mapping, Case Study Borneo. Available online: <https://library.wur.nl/WebQuery/wurpubs/fulltext/50976> (accessed on 3 November 2021).
92. Saradjian, M.; Hosseini, M. Soil moisture estimation by using multipolarization SAR image. *Adv. Space Res.* **2011**, *48*, 278–286. [[CrossRef](#)]
93. Yadav, V.P.; Prasad, R.; Bala, R. Leaf area index estimation of wheat crop using modified water cloud model from the time-series SAR and optical satellite data. *Geocarto Int.* **2019**, *36*, 791–802. [[CrossRef](#)]
94. Satalino, G.; Mattia, F.; Balenzano, A.; Panciera, R.; Walker, J.; Walker, J. Soil moisture maps from time series of PALSAR-1 scansar data over Australia. In Proceedings of the 2013 IEEE International Geoscience and Remote Sensing Symposium—IGARSS, Melbourne, VIC, Australia, 21–26 July 2013; pp. 719–722. [[CrossRef](#)]
95. Najib, N.E.M.; Kanniah, K.D.; Cracknell, A.P.; Yu, L. Synergy of Active and Passive Remote Sensing Data for Effective Mapping of Oil Palm Plantation in Malaysia. *Forests* **2020**, *11*, 858. [[CrossRef](#)]
96. Mathur, R.K.; Suresh, K.; Bhanusri, A.; Naveen, K.P.; Prasad, M.V.; Rao, B.N.; Kalidas, P. *Research Highlights 2011–2015*; ICAR-Indian Institute of Oil Palm Research: Andhra Pradesh, India, 2017; pp. 1–64.
97. Beets, P.N.; Reutebuch, S.; Kimberley, M.O.; Oliver, G.R.; Pearce, S.H.; McGaughey, R.J. Leaf Area Index, Biomass Carbon and Growth Rate of Radiata Pine Genetic Types and Relationships with LiDAR. *Forests* **2011**, *2*, 637–659. [[CrossRef](#)]
98. Gherboudj, I.; Magagi, R.; Berg, A.A.; Toth, B. Soil moisture retrieval over agricultural fields from multi-polarized and multi-angular RADARSAT-2 SAR data. *Remote Sens. Environ.* **2011**, *115*, 33–43. [[CrossRef](#)]
99. Zribi, M.; Baghdadi, N.; Holah, N.; Fafin, O.; Guérin, C. Evaluation of a rough soil surface description with ASAR-ENVISAT radar data. *Remote Sens. Environ.* **2005**, *95*, 67–76. [[CrossRef](#)]